

**CO<sub>2</sub> Hydrogenation**

# A High Pressure *Operando* Spectroscopy Examination of Bimetal Interactions in ‘Metal Efficient’ Palladium/In<sub>2</sub>O<sub>3</sub>/Al<sub>2</sub>O<sub>3</sub> Catalysts for CO<sub>2</sub> Hydrogenation

Matthew E. Potter,\* Sofia Mediavilla Madrigal, Emma Campbell, Lisa J. Allen, Urvashi Vyas, Stephen Parry, Adrián García-Zaragova, Luis M. Martínez-Prieto, Pascual Oña-Burgos, Mads Lützen, Christian D. Damsgaard, Enrique Rodríguez-Castellón, Nicola Schiaroli,\* Giuseppe Fornasari, Patricia Benito,\* and Andrew M. Beale\*

**Abstract:** CO<sub>2</sub> hydrogenation to methanol has the potential to serve as a sustainable route to a wide variety of hydrocarbons, fuels and plastics in the quest for net zero. Synergistic Pd/In<sub>2</sub>O<sub>3</sub> (Palladium on Indium Oxide) catalysts show high CO<sub>2</sub> conversion and methanol selectivity, enhancing methanol yield. The identity of the optimal active site for this reaction is unclear, either as a Pd–In alloy, proximate metals, or distinct sites. In this work, we demonstrate that metal-efficient Pd/In<sub>2</sub>O<sub>3</sub> species dispersed on Al<sub>2</sub>O<sub>3</sub> can match the performance of pure Pd/In<sub>2</sub>O<sub>3</sub> systems. Further, we follow the evolution of both Pd and In sites, and surface species, under *operando* reaction conditions using X-ray Absorption Spectroscopy (XAS) and infrared (IR) spectroscopy. In doing so, we can determine both the nature of the active sites and the influence on the catalytic mechanism.

To reach net zero targets, an extra 10 gigatons of CO<sub>2</sub> must be captured annually,<sup>[1]</sup> thus, there are many opportunities to utilise CO<sub>2</sub>, such as hydrogenation to methanol.<sup>[2]</sup> Most literature focuses on the commercial syngas-to-methanol Cu/

ZnO/Al<sub>2</sub>O<sub>3</sub> catalyst, the industrial catalyst of choice<sup>[3]</sup> which suffers from high CO selectivity at high temperatures. Large quantities of Cu are also required (>30 wt%), which are prone to sintering, limiting lifetime.<sup>[4]</sup> Indium oxide shows

[\*] Dr. M. E. Potter, L. J. Allen, U. Vyas, Prof. A. M. Beale  
 Chemistry Department  
 University College London  
 20 Gordon Street, London, WC1H 0AJ (UK)  
 E-mail: m.potter@ucl.ac.uk  
 andrew.beale@ucl.ac.uk

Dr. M. E. Potter, S. Mediavilla Madrigal, Dr. E. Campbell, L. J. Allen,  
 U. Vyas, Prof. A. M. Beale  
 UK Catalysis Hub  
 Research Complex at Harwell  
 Rutherford Appleton Laboratory, Didcot, OX11 0FA (UK)

S. Mediavilla Madrigal, Dr. E. Campbell  
 Cardiff Catalysis Institute  
 School of Chemistry, Cardiff University, Cardiff, CF10 3AT (UK)

Dr. S. Parry  
 Diamond Light Source  
 Rutherford Appleton Laboratory  
 Didcot, OX11 0FA (UK)

A. García-Zaragova, Dr. L. M. Martínez-Prieto, Dr. P. Oña-Burgos  
 ITQ, Instituto de Tecnología Química  
 Universitat Politècnica de València-Consejo Superior de Investiga-  
 ciones Científicas (UPV-CSIC),  
 Av. de los Naranjos  
 S/N 46022, Valencia (Spain)

Dr. L. M. Martínez-Prieto  
 IIQ, Instituto de Investigaciones Químicas, CSIC-Universidad de  
 Sevilla  
 Departamento de Química Inorgánica; Avda  
 Americo Vespucio 49, 41092 Seville (Spain)

M. Lützen, Dr. C. D. Damsgaard  
 National Centre for Nanofabrication and Characterisation  
 Technical University of Denmark  
 Fysikvej Building 307, 2800 Kgs. Lyngby (Denmark)

Dr. C. D. Damsgaard  
 Department of Physics  
 Technical University of Denmark  
 Fysikvej Building 311, 2800 Kgs. Lyngby (Denmark)

Prof. E. Rodríguez-Castellón  
 Departamento de Química Inorgánica  
 Universidad de Málaga  
 Facultad de Ciencias. 29071 Málaga (Spain)

Dr. N. Schiaroli, Dr. G. Fornasari, Dr. P. Benito  
 Dipartimento di Chimica Industriale “Toso Montanari”  
 Università di Bologna  
 Alma Mater Studiorum, Viale Risorgimento 4, 40136, Bologna  
 (Italy)  
 E-mail: patricia.benito3@unibo.it

Dr. G. Fornasari, Dr. P. Benito  
 Center for Chemical Catalysis—C3  
 Università di Bologna  
 Alma Mater Studiorum, Viale Risorgimento 4, 40136, Bologna  
 (Italy)

© 2023 The Authors. Angewandte Chemie International Edition published by Wiley-VCH GmbH. This is an open access article under the terms of the Creative Commons Attribution License, which permits use, distribution and reproduction in any medium, provided the original work is properly cited.

promise, with a higher methanol selectivity than commercial Cu/ZnO/Al<sub>2</sub>O<sub>3</sub>.<sup>[4b,5]</sup> Studies suggest this activity comes from oxygen vacancies on In<sub>2</sub>O<sub>3</sub> surfaces, as identified by a combination of spectroscopic techniques.<sup>[6]</sup> Despite readily activating CO<sub>2</sub>, In<sub>2</sub>O<sub>3</sub> has modest activity, struggling to split H<sub>2</sub> and convert formate (HCOO) to formaldehyde (H<sub>2</sub>CO). Other metals are introduced to improve hydrogen splitting, particularly, combining Pd and In<sub>2</sub>O<sub>3</sub> improves CO<sub>2</sub> activity while maintaining high methanol selectivity.<sup>[7]</sup>

Many have investigated the Pd–In<sub>2</sub>O<sub>3</sub> synergy, debating the occurrence and role of PdIn alloys.<sup>[4a,7–8]</sup> Pd/In<sub>2</sub>O<sub>3</sub> species, where PdIn was the primary crystalline phase, routinely outperformed monometallic analogues, suggesting a link between PdIn alloys and catalytic activity.<sup>[7b]</sup> PdIn/SiO<sub>2</sub> species also show the presence of PdIn and Pd<sub>2</sub>In<sub>3</sub> phases, depending on the Pd:In ratio, with In Extended X-ray Absorption Fine Structure (EXAFS) spectroscopy confirming over 80% of In formed an alloy.<sup>[7c]</sup> Others demonstrated, with EXAFS, that the synthetic method influences PdIn phase formation, with co-precipitation creating stable PdIn clusters but dry-impregnation causing Pd sintering and lower methanol yields.<sup>[4a]</sup> Similarly, computational work shows that the precise PdIn surface also influences catalytic activity.<sup>[4a,8b,9]</sup> It has been reported PdIn alloys hinder activity, particularly on Pd/In<sub>2</sub>O<sub>3</sub>/SBA-15, which attributes decreasing methanol selectivity to PdIn phases. Rui et al. used a peptide-based method to deposit Pd nanoparticles (NPs) onto In<sub>2</sub>O<sub>3</sub>, where diffraction and XPS (X-ray Photoelectron Spectroscopy) confirmed alloying, concluding that PdIn alloys hindered Pd's hydrogen splitting ability.<sup>[7a,8d]</sup> Significant debate remains on Pd/In<sub>2</sub>O<sub>3</sub> systems, where the large In<sub>2</sub>O<sub>3</sub> quantities encourage alloying, potentially leading to ineffective 'spectator species'. In our system, we limit the metal quantity, supporting Pd and In<sub>2</sub>O<sub>3</sub> onto alumina, making a ternary Pd/In<sub>2</sub>O<sub>3</sub>/Al<sub>2</sub>O<sub>3</sub> species (1 wt% Pd, 12 wt% In<sub>2</sub>O<sub>3</sub>). Al<sub>2</sub>O<sub>3</sub> was chosen as a robust oxidic support to firmly anchor Pd and In<sub>2</sub>O<sub>3</sub> to the catalyst. Due to the lower loading in our systems, the formation of alloys will be more evident using EXAFS.<sup>[8d]</sup> While ex situ and *in situ* studies provide valuable indirect evidence and descriptors for catalytic activity, *operando* spectroscopy identifies active sites in the reaction (Figures S1 to S3 & Table S1).<sup>[6c,10]</sup> This is vital for elevated temperatures with pressures, reactive atmospheres, etc. which can trigger phase changes, and potential alloying.

Our Pd/In<sub>2</sub>O<sub>3</sub>/Al<sub>2</sub>O<sub>3</sub> contains less In<sub>2</sub>O<sub>3</sub> than undeposited Pd/In<sub>2</sub>O<sub>3</sub> but has similar activity (Figure S4), with improved methanol selectivity (Figure S4B, remaining selectivity is CO), making them of significant interest for CO<sub>2</sub> utilisation.<sup>[11]</sup> High-resolution Transmission Electron Microscopy (HRTEM) and Scanning Transmission Electron Microscopy–High-Angle Annular Dark Field Imaging (STEM-HAADF) of spent Pd/In<sub>2</sub>O<sub>3</sub>/Al<sub>2</sub>O<sub>3</sub> show an average particle size of 1.3 ± 0.3 nm and STEM/Electron Energy Loss Spectroscopy (STEM/EELS) maps show regions of overlapping Pd and In, suggesting intimate mixing (Figure S5). XPS of the calcined system suggests (Figure S6) In is present as In<sub>2</sub>O<sub>3</sub>, with and without Pd, with a Pd 3d<sub>5/2</sub> peak at 444.8 eV. Similarly, Pd XPS showed identical signals in

Pd/Al<sub>2</sub>O<sub>3</sub> and Pd/In<sub>2</sub>O<sub>3</sub>/Al<sub>2</sub>O<sub>3</sub>.<sup>[7a,12]</sup> Initial EXAFS data suggests that the Pd exists as PdO, whereas In exists as In<sub>2</sub>O<sub>3</sub> (Figure 1).

To explore the Pd and In environments, and possible interactions, EXAFS spectra were collected during reduction (Figures 1 & 2), and CO<sub>2</sub> hydrogenation at 20 bar (Figures 2 & 3). Pd NPs are susceptible to aerial oxidation, so *in situ* and *operando* measurements are needed for genuine insight into active, reactive species. Collecting both In and Pd EXAFS allows changes to be correlated, probing bimetallic interactions. This is complemented by high-pressure *operando* Diffuse Reflectance Infrared Fourier Transform Spectroscopy (DRIFTS), following similar conditions as the EXAFS. DRIFTS data will help to elucidate the catalytic mechanism, and synergistic enhancement, in the Pd/In<sub>2</sub>O<sub>3</sub>/Al<sub>2</sub>O<sub>3</sub> system.

EXAFS data (Figure 1A) initially shows PdO, as expected following calcination, transforming to Pd(0) on reduction, with a noticeable decrease in the rising absorption edge intensity and position (Figure S7 & S8).<sup>[13]</sup> Our XANES (X-ray Absorption Near-Edge Structure) data shows the Pd-edge lowering in energy on reduction, confirming the Pd is being reduced, moving to a similar energy to reduced Pd/Al<sub>2</sub>O<sub>3</sub> and Pd foil (Figures S7 & S8). R-space EXAFS shows a decrease in the Pd–O path (1.54 Å

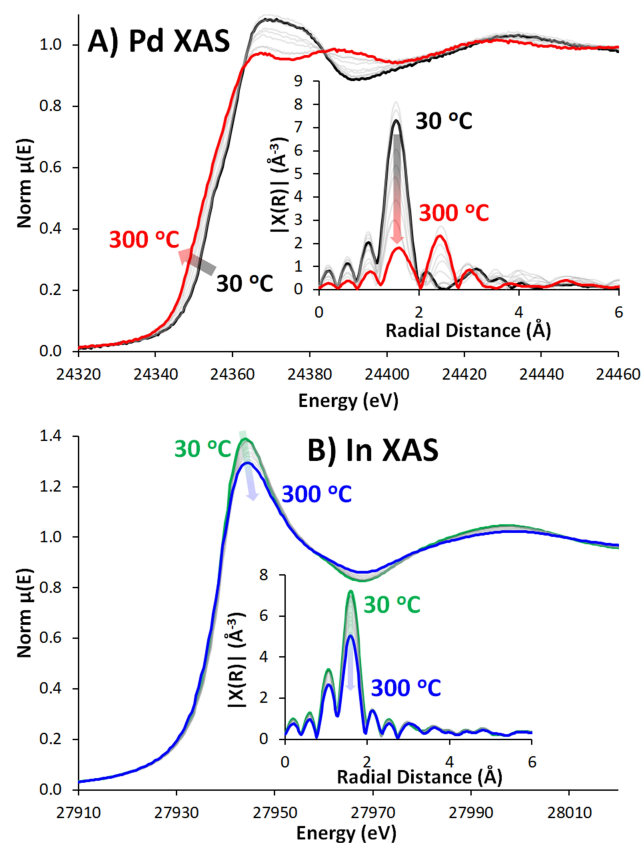


**Figure 1.** Evolution of Pd and In XAS (X-ray Absorption Spectroscopy) data of Pd/In<sub>2</sub>O<sub>3</sub>/Al<sub>2</sub>O<sub>3</sub> during *in situ* reduction, with increasing reduction temperature, showing near-edge, and insets of R-space plot for A) Pd K-edge and B) In K-edge.

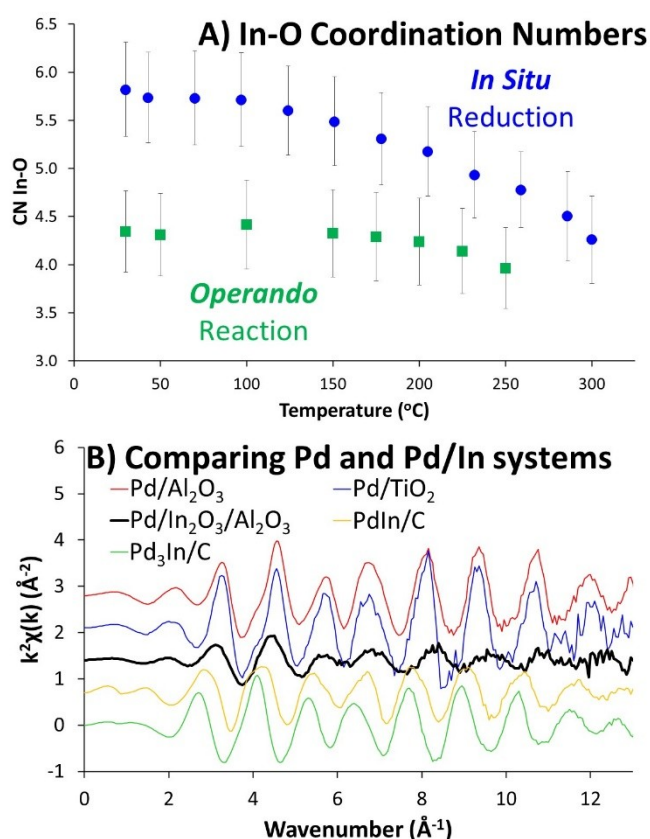


**Figure 2.** A) Progression of In–O CN during *in situ* reduction and *operando* reaction as temperature increases, and B) Comparing *k*-space plots of monometallic and alloyed PdIn systems with our Pd/In<sub>2</sub>O<sub>3</sub>/Al<sub>2</sub>O<sub>3</sub> species.

radial distance) and an emerging Pd–Pd path at 2.45 Å (Figure 1A). EXAFS and LCF (Linear Combination Fitting) data suggest our system may not be fully reduced, with a small quantity of oxidic character remaining (Figures 1A & S8). Given the small size of our Pd systems (1.3 nm), it is possible the remaining PdO character is due to interactions between surface metallic Pd atoms and the oxidic Al<sub>2</sub>O<sub>3</sub>, or In<sub>2</sub>O<sub>3</sub> components. If so, such species are unlikely to be accessible to our reagents. The *in situ* Pd reduction EXAFS data was not fitted, as the combination of changing temperature (varying Debye–Waller factors), with varying amounts of two different Pd environments (metallic and oxidic) means many variables must be calculated. Attempts to do this led to a significant increase in error estimation but simply supported the findings already observed by the XANES findings (Figures 1A, S7 & S8) that there was an increase in metallic character and a reduction in oxidic phase.

Initially, In exists as In<sub>2</sub>O<sub>3</sub>. As temperature increases, the oscillations dampen, and the pre-edge energy slightly decreases (Figures 1B & S9).<sup>[6c]</sup> LCF analysis suggests a small quantity of In is reduced, though the position of the rising absorption edge shows no discernible movement, suggesting no significant redox occurs (Figure S10). R-space plots show a strong In–O signal (Figure 1B), which

decreases with increased temperature. Notably, there is no evidence of a metallic In–In signal ( $\approx 3.0$  Å) or In–Pd signal ( $\approx 2.5$  Å).<sup>[7c]</sup> The lack of In–In signal (Figure S11, Table S2) is jointly attributed to In<sub>2</sub>O<sub>3</sub> existing as small nanoparticles, and the amorphous nature of the In<sub>2</sub>O<sub>3</sub> in our system, as seen by powder X-ray diffraction (Figure S11B). Both factors limit long-range order and crystallinity for In<sub>2</sub>O<sub>3</sub>, leading to greatly reduced intensity for subsequent shells. This is likely different to pure In<sub>2</sub>O<sub>3</sub> or binary Pd/In<sub>2</sub>O<sub>3</sub> systems, where there is significantly more In<sub>2</sub>O<sub>3</sub>, leading to larger particle sizes, that typically adopt a crystalline bixbyite structure.<sup>[4a]</sup> The absence of an In–Pd signal in the In EXAFS further suggests the 2.45 Å signal in the Pd EXAFS is Pd–Pd, and not Pd–In, as Pd–In signals should be expected in both Pd and In EXAFS data.

The decreasing In–O signal is likely from oxygen vacancies forming, aligning with the CN (Coordination Number) decreasing from 5.8 (30°C) to 4.3 (300°C; Figure 2A & Table S2), and also possibly from increasing thermal disorder. The strong correlation between the Debye–Waller factor (thus, temperature) and coordination number is a constant challenge in EXAFS fitting. To eliminate thermal effects influencing the In–O CN, In EXAFS spectra at 30°C were compared pre- and post-reduction, confirming a reduction of CN beyond error (Figure 2A, Table S3), supporting oxygen vacancy formation. This is further evidenced by the change in pre-edge energy, implying a decrease in the overall oxidation state (Figure S9). Furthermore, the In–O bond length shortens from 2.13 to 2.10 Å (Table S3 & Figure S11A), as In forms stronger bonds with remaining oxygen ions. Thus, PdO reduces to Pd metal, whilst In<sub>2</sub>O<sub>3</sub> forms oxygen vacancies with no significant evidence of alloying.

To investigate possible alloying, EXAFS data of Pd/In<sub>2</sub>O<sub>3</sub>/Al<sub>2</sub>O<sub>3</sub> was compared with monometallic 1 wt% Pd/Al<sub>2</sub>O<sub>3</sub> and 5 wt% Pd/TiO<sub>2</sub> species, along with alloyed bimetallic PdIn/C and Pd<sub>3</sub>In/C species, where the alloying was confirmed with powder XRD (X-ray Diffraction; Figure S12). The XANES region (Figure S13) shows the EXAFS peaks of Pd/In<sub>2</sub>O<sub>3</sub>/Al<sub>2</sub>O<sub>3</sub> differ from both monometallic and bimetallic species, though they more closely match the monometallic species. This is reinforced by the *k*-space plots (Figure 2B & S14), where the oscillations of the Pd/In<sub>2</sub>O<sub>3</sub>/Al<sub>2</sub>O<sub>3</sub> species align well with the monometallic species but differ from the bimetallic PdIn/C and Pd<sub>3</sub>In/C species. This provides further evidence that Pd and In, in Pd/In<sub>2</sub>O<sub>3</sub>/Al<sub>2</sub>O<sub>3</sub>, are likely distinct monometallic species. On fitting (Table S3), there was no evidence of a Pd–In feature in the Pd/In<sub>2</sub>O<sub>3</sub>/Al<sub>2</sub>O<sub>3</sub> system. The alloyed bimetallic species had a notably longer Pd–Metal (Pd–In here) bond length (both 2.78 Å) than the two monometallic species (2.73 and 2.74 Å). The Pd–M (Pd–Pd) bond length of the Pd/In<sub>2</sub>O<sub>3</sub>/Al<sub>2</sub>O<sub>3</sub> is smaller than all other systems (2.64 Å) observed, though closer to the monometallic species. While this is shorter than typical Pd–Pd bonds<sup>[14]</sup> and likely due to their small size. Overall, comparing these model systems suggests that Pd/In<sub>2</sub>O<sub>3</sub>/Al<sub>2</sub>O<sub>3</sub> does not show significant signs of alloying, providing more evidence that Pd and In<sub>2</sub>O<sub>3</sub> exist as distinct sites, and not as an alloy.

Post reduction, the cooled system was pressurised to 20 bar. Spectra were collected from 30 to 250 °C (Figure 3), while mass-spec (MS) data from the outlet confirms methanol concentration ( $m/z$  31, Figure S15) increasing above 200 °C, showing the catalyst performs CO<sub>2</sub> hydrogenation under *operando* conditions. During the reaction, fitted Pd EXAFS (Table S4) showed there was little change (Figure 3A), confirmed by LCF analysis and the energy position of the rising absorption edge (Figures 2A & S16). R-space EXAFS showed a subtle variation in the Pd–O and Pd–Pd path intensities (Figure 3A). Changes in CN and bond length were within error (Table S4 & Figures S17 & S18). In also shows little change during the catalytic reaction. The pre-edge and rising absorption edge energies show minimal variation, whilst there is a subtle dampening of the EXAFS oscillations, typically due to the increase in sample temperature (Figure 3B).

LCF analysis shows a slight decrease in In<sub>2</sub>O<sub>3</sub> character from 50 °C to 250 °C, but there is little correlation with the line energy as temperature changes, suggesting no significant variation in oxidation state (Figure S19). In–O CN changes from 4.3 to 4.0 (Table S5 & Figure 2A), reflecting the decreased intensity in the R-space plot, but this, and differing In–O bond lengths, are within error (Figure S20).

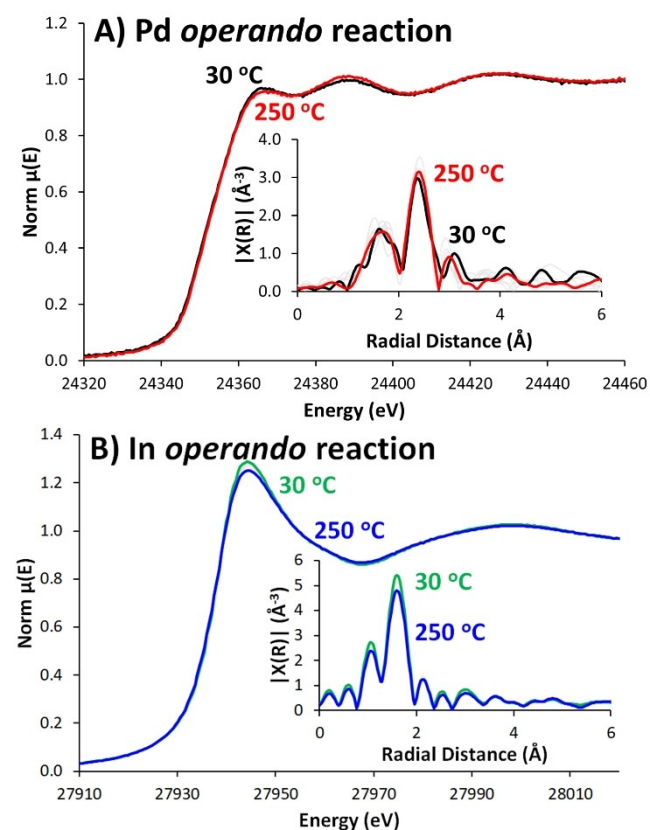


**Figure 3.** Evolution of Pd and In EXAFS data of Pd/In<sub>2</sub>O<sub>3</sub>/Al<sub>2</sub>O<sub>3</sub> during *operando* reduction, as a function of increasing reaction temperature, showing XANES progression with insets showing R-space plot for A) Pd K-edge and B) In K-Edge.

This suggests oxygen vacancies are retained, as the system remains in a primarily reducing atmosphere.

*Operando* EXAFS shows little change from the post-reduction state, suggesting the state after *in situ* reduction step is a reasonable representation of the actual active species. No significant evidence of alloying, or PdIn phases was found, unlike in Pd/In<sub>2</sub>O<sub>3</sub> species, where contact between Pd and In<sub>2</sub>O<sub>3</sub> is ensured. This does, however, not preclude contact between the Pd and In<sub>2</sub>O<sub>3</sub> phases, or Pd–O–In species in these systems.

*Operando* DRIFTS at 1 and 20 bar explored the Pd–In<sub>2</sub>O<sub>3</sub> synergy and reaction mechanism (Table S6, Figures S21 to S26). In<sub>2</sub>O<sub>3</sub>/Al<sub>2</sub>O<sub>3</sub> at 1 bar (Figure S21) shows a rapid loss of polydentate carbonates (1672 cm<sup>-1</sup>) up to 175 °C, coinciding with formate appearance (1606, 1392 and 1305 cm<sup>-1</sup>), and unidentate carbonates (1519 cm<sup>-1</sup>).<sup>[15]</sup> The C–H region is dominated by formate bands (2994, 2902 and 2740 cm<sup>-1</sup>), with a methoxy shoulder (2923 cm<sup>-1</sup>).<sup>[15]</sup> At 20 bar (Figure S22), the carbonate region of In<sub>2</sub>O<sub>3</sub>/Al<sub>2</sub>O<sub>3</sub> is dominated by gaseous rotational bands, though growing formate bands are discernible. At 20 bar, formates still evolve with temperature, but methoxy (2960 & 2852 cm<sup>-1</sup>) and methane formation (3015 cm<sup>-1</sup> and associated rotational bands) occurs, which is attributed to the DRIFTS cell itself, as these were also seen in an identical experiment with KBr instead of the catalyst.<sup>[15]</sup> No CO bands were observed, suggesting In<sub>2</sub>O<sub>3</sub> follows the formate pathway.<sup>[5,6b]</sup> The continually increasing formate signals suggest the rate determining step of the reaction is formate reduction, with In<sub>2</sub>O<sub>3</sub>/Al<sub>2</sub>O<sub>3</sub> being an inefficient hydrogen activator, due to the continual presence of activated CO<sub>2</sub> species, and slower formate production, causing lower methanol yields (Figure S4). Pd/Al<sub>2</sub>O<sub>3</sub> shows CO formation at 1 bar (2030 and broad 1890 cm<sup>-1</sup>, Figure S20) due to Reverse-Water-Gas Shift (RWGS). At 1 bar, carbonate species decrease rapidly in Pd/Al<sub>2</sub>O<sub>3</sub>, suggesting improved conversion. The C–H region shows a rapid formate increase until 175 °C, where it decreases as methoxy signals appear (2910 cm<sup>-1</sup>, Figure S23). Aside from rotational bands, the 20 bar and 1 bar Pd/Al<sub>2</sub>O<sub>3</sub> spectra are similar (Figure S24), except the CO feature decreases with temperature. The C–H region shows the formate signals behaving like the 1 bar system, though signals due to methane (3016 cm<sup>-1</sup>) and methanol are present.<sup>[15]</sup>

Comparing the 1 and 20 bar spectra suggests pressure has little influence on formate formation but improves methoxy and methanol formation. At 1 and 20 bar, the formate species plateau at 175 °C, thus are converted, regardless of pressure. This may be because adsorbed CO<sub>2</sub> favours RWGS, or more rapid hydrogen activation, readily converting the formate species. Ineffective Pd/Al<sub>2</sub>O<sub>3</sub> performance is likely due to sluggish CO<sub>2</sub> activation, as any activated species (formate) are rapidly removed. At 1 bar, Pd/In<sub>2</sub>O<sub>3</sub>/Al<sub>2</sub>O<sub>3</sub> resembles the In<sub>2</sub>O<sub>3</sub>/Al<sub>2</sub>O<sub>3</sub> system, with formate continually present, though also some CO (2042 cm<sup>-1</sup>, Figure 4A, S25 & S26). The C–H region shows continuous formate growth, with a discernible methoxy shoulder (2842 cm<sup>-1</sup>) above 250 °C. At 20 bar, Pd/In<sub>2</sub>O<sub>3</sub>/Al<sub>2</sub>O<sub>3</sub> is again similar to In<sub>2</sub>O<sub>3</sub>/Al<sub>2</sub>O<sub>3</sub>, with a pronounced

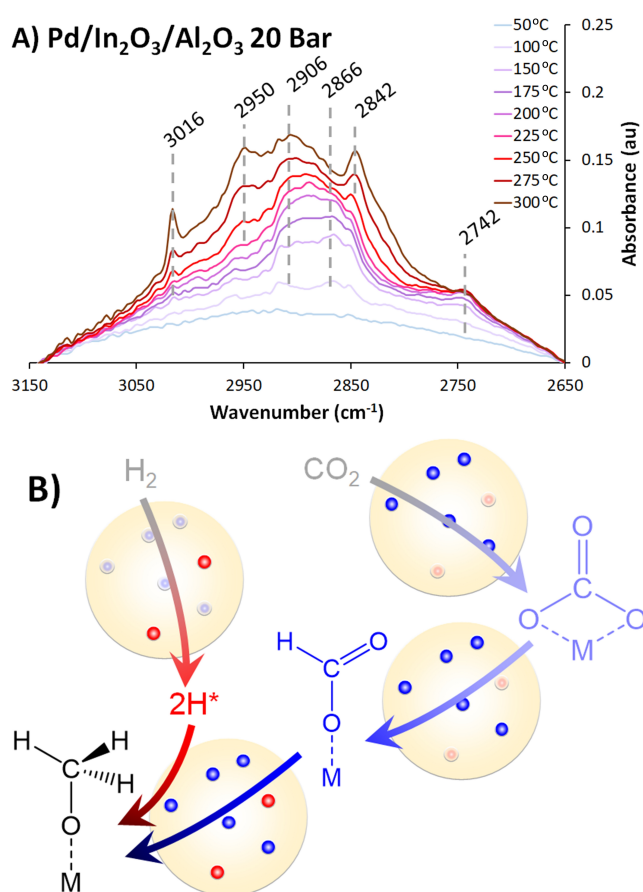


**Figure 4.** A) Operando DRIFTS difference spectra of Pd/In<sub>2</sub>O<sub>3</sub>/Al<sub>2</sub>O<sub>3</sub>, with 30 mL/min of 75% H<sub>2</sub> and CO<sub>2</sub>, under 20 Bar of pressure and B) mechanistic implications with Pd represented as red circles, and In<sub>2</sub>O<sub>3</sub> as blue circles.

increase in formate features (1618, 1394 and 1313 cm<sup>-1</sup>), peaking at 250°C.<sup>[15]</sup> CO signals are lower than Pd/Al<sub>2</sub>O<sub>3</sub>, suggesting RWGS is less effective, with the formate pathway dominating. This agrees with the C–H stretch region, where formate species transition to methanol and methoxy species, suppressing methane formation. Comparing the mono and bimetallic systems suggests that hydrogen and CO<sub>2</sub> activations occur more optimally. In<sub>2</sub>O<sub>3</sub>/Al<sub>2</sub>O<sub>3</sub> continually creates formate, with little methanol or methoxy, as the oxygen vacancies readily activate CO<sub>2</sub>. Pd/Al<sub>2</sub>O<sub>3</sub> rapidly depleted formate, suggesting hydrogen activation surpassed CO<sub>2</sub> activation. Pd/In<sub>2</sub>O<sub>3</sub>/Al<sub>2</sub>O<sub>3</sub> increases formate presence up to 250°C, and noticeably transitions to strong methanol and methoxy signals (Figures 4B and S28).

Based on the above findings, we suggest that Pd–In synergy in these systems comes from two sites separately performing individual functions (hydrogen and CO<sub>2</sub> activation, respectively). Subtle changes occur under reaction conditions which may evidence delicate Pd–In<sub>2</sub>O<sub>3</sub> interactions (i.e., suppressing reverse water gas shift activity), though no *significant* alloying occurs nor appears to be necessary for improved methanol yield (Figure S4). These findings suggest that careful balancing of individual CO<sub>2</sub> and

hydrogen activation processes, and the precise location and interactions of Pd and In<sub>2</sub>O<sub>3</sub>, are key to future catalyst optimisation. Likely extending beyond Pd/In<sub>2</sub>O<sub>3</sub> systems to other bimetallic CO<sub>2</sub> hydrogenation systems.

### Acknowledgements

UK Catalysis Hub is kindly thanked for resources and support provided via the membership of the UK Catalysis Hub Consortium and funded by current EPSRC grants: EP/R026939/1 and EP/R026815/1. We thank Diamond Light Source for provision of beam time and support facilities at the beamline B18, under proposal SP30647. We also acknowledge the European Synchrotron Radiation Facility (ESRF) for provision of synchrotron radiation facilities and we would like to thank Dragos Stoian, Kenneth Marshall, Wouter van Beek and Naomi Lawes for assistance and support in using beamline BM31. This project has received funding from the European Union's Horizon 2020 research and innovation programme under grant agreement No 101022507. This work was supported by a research grant (9455) from VILLUM FONDEN. ERC and PBM wish to thank the Spanish Ministry of Science and Innovation, for projects PID2021-126235OB-C32 and TED2021-130756B-C31 funded by MCIN/AEIMCIN/AEI/10.13039/501100011033 and FEDER funds, and by "ERDF A way of making Europe, respectively". We thank Elena Rodríguez Aguado for performing XPS measurements.

### Conflict of Interest

The authors declare no conflict of interest.

### Data Availability Statement

The data that support the findings of this study are available from the corresponding author upon reasonable request.

**Keywords:** CO<sub>2</sub> Utilization · Catalysis · EXAFS · Operando · Spectroscopy

- [1] *Negative Emissions Technologies and Reliable Sequestration: A Research Agenda*, The National Academies Press, Washington, DC, 2019.
- [2] A. Goepfert, M. Czaun, J. P. Jones, G. K. Surya Prakash, G. A. Olah, *Chem. Soc. Rev.* **2014**, *43*, 7995–8048.
- [3] a) M. Behrens, F. Studt, I. Kasatkin, S. Kuhl, M. Havecker, F. Abild-Pedersen, S. Zander, F. Girgsdies, P. Kurr, B. L. Kniep, M. Tovar, R. W. Fischer, J. K. Norskov, R. Schlogl, *Science* **2012**, *336*, 893–897; b) D. Laudenschleger, H. Ruland, M. Muhler, *Nat. Commun.* **2020**, *11*, 3898.
- [4] a) M. S. Frei, C. Mondelli, R. Garcia-Muelas, K. S. Kley, B. Puertolas, N. Lopez, O. V. Safonova, J. A. Stewart, D. Curulla Ferre, J. Perez-Ramirez, *Nat. Commun.* **2019**, *10*, 3377; b) O. Martin, A. J. Martin, C. Mondelli, S. Mitchell, T. F.

- Segawa, R. Hauert, C. Drouilly, D. Curulla-Ferre, J. Perez-Ramirez, *Angew. Chem. Int. Ed.* **2016**, *55*, 6261–6265.
- [5] J. Wang, G. Zhang, J. Zhu, X. Zhang, F. Ding, A. Zhang, X. Guo, C. Song, *ACS Catal.* **2021**, *11*, 1406–1423.
- [6] a) A. Cao, Z. Wang, H. Li, J. K. Nørskov, *ACS Catal.* **2021**, *11*, 1780–1786; b) P. Gao, S. Li, X. Bu, S. Dang, Z. Liu, H. Wang, L. Zhong, M. Qiu, C. Yang, J. Cai, W. Wei, Y. Sun, *Nat. Chem.* **2017**, *9*, 1019–1024; c) A. Tsoukalou, P. M. Abdala, D. Stoian, X. Huang, M. G. Willinger, A. Fedorov, C. R. Muller, *J. Am. Chem. Soc.* **2019**, *141*, 13497–13505.
- [7] a) N. Rui, Z. Wang, K. Sun, J. Ye, Q. Ge, C.-J. Liu, *Appl. Catal. B* **2017**, *218*, 488–497; b) A. García-Trenco, A. Regoutz, E. R. White, D. J. Payne, M. S. P. Shaffer, C. K. Williams, *Appl. Catal. B* **2018**, *220*, 9–18; c) J. L. Snider, V. Streibel, M. A. Hubert, T. S. Choksi, E. Valle, D. C. Upham, J. Schumann, M. S. Duyar, A. Gallo, F. Abild-Pedersen, T. F. Jaramillo, *ACS Catal.* **2019**, *9*, 3399–3412.
- [8] a) G. Tian, Y. Wu, S. Wu, S. Huang, J. Gao, *Catal. Lett.* **2023**, *153*, 903–910; b) P. Wu, B. Yang, *Catal. Sci. Technol.* **2019**, *9*, 6102–6113; c) H. Jiang, J. Lin, X. Wu, W. Wang, Y. Chen, M. Zhang, *J. CO<sub>2</sub> Util.* **2020**, *36*, 33–39; d) J. Ye, Q. Ge, C.-J. Liu, *Chem. Eng. Sci.* **2015**, *135*, 193–201.
- [9] J. Ye, C.-J. Liu, D. Mei, Q. Ge, *J. Catal.* **2014**, *317*, 44–53.
- [10] a) I. Lezcano-Gonzalez, R. Oord, M. Rovezzi, P. Glatzel, S. W. Botchway, B. M. Weckhuysen, A. M. Beale, *Angew. Chem. Int. Ed.* **2016**, *55*, 5215–5219; b) J. J. Sattler, A. M. Beale, B. M. Weckhuysen, *Phys. Chem. Chem. Phys.* **2013**, *15*, 12095–12103.
- [11] N. Schiaroli, L. Negahdar, M. Lützen, P. Hoang Ho, L. J. Allen, A. Natoli, F. Ospitali, F. Maluta, E. Rodríguez-Castellón, C. D. Damsgaard, G. Fornasari, A. M. Beale, P. Benito, *J. Catal.* **2023**, *424*, 140–151.
- [12] M. Chen, J. Xu, Y. Cao, H.-Y. He, K.-N. Fan, J.-H. Zhuang, *J. Catal.* **2010**, *272*, 101–108.
- [13] P. Lott, P. Dolcet, M. Casapu, J.-D. Grunwaldt, O. Deutschmann, *Ind. Eng. Chem. Res.* **2019**, *58*, 12561–12570.
- [14] D. Decarolis, A. H. Clark, T. Pellegrielli, M. Nachtegaal, E. W. Lynch, C. R. A. Catlow, E. K. Gibson, A. Goguet, P. P. Wells, *ACS Catal.* **2021**, *11*, 2141–2149.
- [15] a) T. Das, G. Deo, *J. Mol. Catal. A* **2011**, *350*, 75–82; b) A. Kaftan, M. Kusche, M. Laurin, P. Wasserscheid, J. Libuda, *Appl. Catal. B* **2017**, *201*, 169–181; c) W. Wang, Z. Qu, L. Song, Q. Fu, *J. Catal.* **2020**, *382*, 129–140.

Manuscript received: August 28, 2023

Accepted manuscript online: September 18, 2023

Version of record online: September 29, 2023